Received: 25 June 2022 | Revised: 14 July 2022 | Accepted: 21 July 2022
DOI: 10.22034/ecc.2022.348852.1494
Eurasian Chemical Communications
SAMI

FULL PAPER

Synthesis and characterization of some metal complexes with 2,6-bis(((1-octyl-1H-1,2,3-triazol-4-yl) methoxy) methyl) pyridine and the study of their biological activities

Jihan Hameed Abdulameer[a,*] | Mahasin F. Alias[b]

[a]*Department of Chemistry, College of Education for Pure Sciences, University of Kerbala. Kerbala, Iraq*

[b]*Department of Chemistry, College of Science for Women, University of Baghdad, Baghdad, Iraq*

In this work, the chelation reaction was investigated between 2,6-bis((1-octyl-1H-1,2,3-triazole-4-yl)methoxy)methyl)pyridine (L) as organic chelating with metal ions Mn2+, Pd2+, and Au3+ to form various novel complexes. The organic ligand was synthesized by using click reaction between 1-azidooctane and 2,6-bis((prop-2-yn-1-yloxy) methyl) pyridine (triazole derivative), the mentioned reaction was catalyzed by Cu(I) ion. All structures of these new compounds were rigorously characterized by spectroscopic methods such as in the solid and solution states as 1HNMR, 13CNMR, Uv-Vis, FTIR, Mass spectrometry, metal and elemental analyses, magnetic susceptibility, and conductivity measurements at room temperature. Through the diagnosis, we concluded that the ligand may behave as a tetradentate and pentdentate chelate. The L-Pd and L-Au complexes have square planer geometry, while the L-Mn complex has octahedral geometry. All prepared compounds were applied to the selected micro-organisms and tested the ability of these compounds to inhibit the bacteria (Staph. aureus, andE. coli) and fungi (cand. andalbicaus) growth, by using three different concentrations (10, 50, and 200) ppm. In general, the results show that the increase in concentration gives more activity as antibacterial and antifungal and that the gold complex was more synergetic effective than others, but especially, the compounds behave as strong antibacterial towards Escherichia coli.

***Corresponding Author:**
Jihan Hameed Abdulameer
Email: Jihan.hameed@uokerbala.edu.iq
Tel.: +9647802268195

KEYWORDS

Biological activity; metal ions; chelation reaction; triazole derivatives.

Introduction

One of the significant types of heterocyclic compounds containing nitrogen atoms is called Triazole, where these compounds have (1,2,3-triazole) and (1,2,4-triazole). The importance of this class is due to several reasons, including their broad range of biological actions, the growing resistance to the conventional antibiotics, their wide range of uses in preparing medicines, antibiotics, nucleosides, tri-tubercular agents, receptors, fluorinated hydrogels, chelators, surface-active agents, and radio-chemistry [1]. An example of a click reaction is the Copper-catalyzed 1,3-Dipolar cycloaddition reaction of azides with terminal alkynes, which is catalyzed by Cu^{+} ion as showed by the study conducted by Sharpless *et al*. Click chemistry is a collection of powerful, highly reliable, and diverse processes for the fast synthesis of significant novel compounds [2,3], this reaction is regioselective, yielding only 1,4-

substituted products. It also produces good yields and is faster by 107 times than the non-catalyzed reaction [4]. In addition to its complexes, several triazole derivatives have been identified as effective chemicals for generating a range of metal coordination structures [5]. Antifungal drugs, plant growth inhibitors, plant protection, chemical photography, biosynthesis inhibitors, and shock therapy are some of the derivatives of triazole [6].

Photoluminescent complexes have attracted a lot of attention, and they are being used in a variety of implementations, such as Lambda sensors, probes for biological activity, and PHOLEDs. Compounds containing cyclic imines are very important in current coordination chemistry for building stabilized metal complexes [7]. In addition to effective antiviral medicines, triazole compounds containing various transition metals demonstrated important antimicrobial and antitumor actions. In comparison with the native ligands and their coordination compounds with S, N-heterocycles show promise to improve biological activity [8].

Lots of complexes examples include triazole ligands such as: Sanaa M. Emam et al. [9] have investigated a series of twelve complexes prepared by reaction of metal ions: Co^{2+}, Ni^{2+}, Cu^{2+}, Zn^{2+}, and Cd^{2+} with 3-(3'-pyridyl)-4-amino-5-mercapto-1,2,4-triazole [HL] that indicate inhibition activities towards the bacteria *S. pyogenes* (Gram positive) and the data revealed that the complex $[Cd(HL)(NO_3)_2(H_2O)].2.25H_2O$. 0.25EtOH is more active than other chelates.

Al-Radadi, N.S *et al*. [10] were used the organic metal of 4-amino-5-heptadecyl-4H-1,2,4-triazole-3-thiol with some light and heavy metal ions (Co^{2+}, Ni^{2+}, Cu^{2+}, Cd^{2+}, and Fe^{3+}) to form the octahedral structure of mononuclear chelates by 2:1 ratio from ligand to metal, all the prepared complexes were characterized by spectral, thermal and physical methods, and the bioassay as antibacterial were applied on these compounds against *B. subtilis* and *S. pyogenes* as $Gram^+$ and *E. coli* and *P. vulgaris* as $Gram^-$. Based on the results, it was noted that there is a difference in effectiveness against using a bacterium, and in general, the compounds showed the highest resistance against *E. coli*.

Another study was done by Mohamed Gaber *et al*. [11] included complexes synthesis from divalent metals [Mn(II), Co(II), and Ni(II)] with azo-ligand based on 3-amino-5-mercapto-1,2,4-triazole. All chelates were tested as DNA-binding, antimicrobial, and anticancer in addition to physio-chemical and theoretical studies. As we know, studying how a molecule interacts with DNA is of great importance in determining the behavior of a compound as a drug. The estimated data show that the Ni-complex was more intensively bound to DNA than others. The antimicrobial activity was tested via various species of bacteria and fungi and demonstrated low and moderate performance compared with the standard drug. While the in-vitro toxicity was evaluated versus liver carcinoma, the results exhibited that Co-complex and Ni-complex, respectively, have more activity than Mn-complex and azo-ligand.

Dipanjan M. and Dr. Maravanji S. B. [12] described various methods to prepare triazoles-based phosphine in their mini-review and show the successfully complexation of these compounds with Pd(II). Many previous and recent studies dealt with many applications of triazole derivatives with metallic elements. In this research, some concepts of click chemistry were depended to prepare the ligand containing triazole moiety and tested as antimicrobial. Scheme 1 shows the graphical abstract of current work.

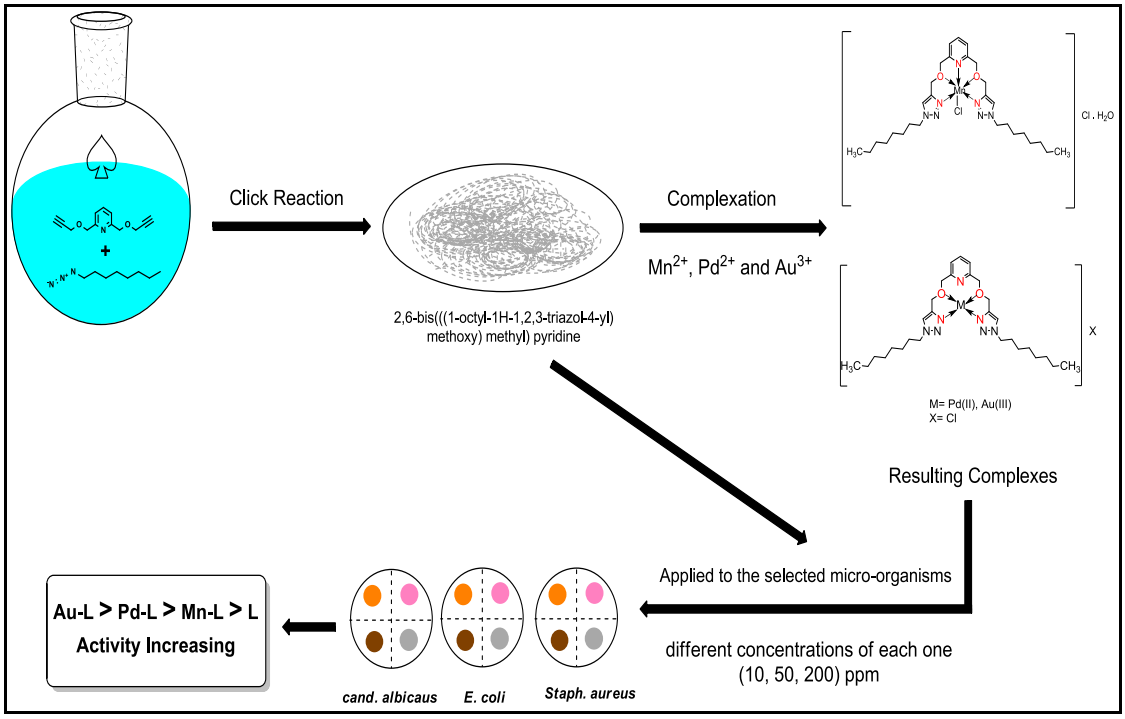

SCHEME 1 Graphical abstract of work

Materials and methods

Materials, physical measurements, and analysis

The chemicals employed in this study were pure grade reagents procured from BDH, Merck, and Sigma-Aldrich in the United States. The Euro EA3000 analyzer was used for the determined (C, H, and N) contents. Bruker DPX spectrometers operating at 600 MHz were used to obtain NMR spectra, with COSY and HSQC supporting NMR assignments of the target compounds. The University of New South Wales in Australia employed the Orbitrap LTQ XL ion trap MS apparatus to acquire HRMS at the mode of the positive ion with an electrospray-ionization (ESI) source. The Agilent spectrometer (FT-IR 8400S SHIMADZU Spectrophotometer) was used to measure FT-IR spectra of the prepared complexes and their ligand in the solid-state at the range of wavenumber at 4000-400 and 4000-200 cm^{-1} by using KBr and CsI pellets. By a Uv-Vis, 1800 PC Shimadzu Spectrophotometer, the electronic spectra were recorded at wave lengths ranging from (1100-190) nm for the prepared complexes and their ligand in solution state. The electrical conductivity meter (WTW) and magnetic susceptibility of complexes was determined at 25 °C. The measurements of melting point of all solid products were determined by GALLEN KAMP M.F.B-60 SMP30/ Stuart apparatus. Thin layer chromatography was employed to adjust the reaction and the silica plates were used (60 F254, 0.2 mm), which carried alkaline potassium permanganate dip.

Synthesis of 2,6-bis(((1-octyl-1H-1,2,3-triazol-4-yl)methoxy)methyl)pyridine [BOTMMP/L]

Preparation of this ligand was carried out according to the following steps (as shown as in Scheme 2) [13]:

A-Synthesis of n-alkyl azides (1-azidooctane) [1-AO]

(99%, 11.18 g, 0.172 mmol) of sodium azide was added to a whiskered solution from 1-Bromooctane (98%, 10 mL) in DMF (99.5%, 70 mL), while continuing to stir the formed suspension at the range of (60-70) °C in a heated oily bath about (5-6) hours, the

mixture of reaction was poured into (140) mL of distilled water, and then it was separated by (99.8%, 350) mL of diethyl ether. Next, the organic layer was collected and washed to form light yellow liquid of 1-azidooctane. After that, it was purified by flash chromatography (silica gel, n-hexane), Rf = 0.82 (n-Hexane) to yield a colorless liquid.

B-Synthesis of 2,6-bis((prop-2-yn-1-yloxy)methyl)pyridine[BPMP]

In a dry flask, (98%, 2.8 g, 20 mmol) of pyridine-2,6-diyldimethanol was dissolved by (98%, 50) mL of DMF with adding up to (98%, 3.2 g, 80 mmol) of crushed NaOH, and before adding propargyl bromide (98%, 3.79 mL, 44 mmol) dropwise, the ice-salt bath was used to cool the round flask in (-20 °C) with agitate the contents for 10 minutes, and then the reaction mixture was stirred for additional 24 hours with progressively heating at room temperature. Later, the reaction was subsided by adding 100 mL of distilled water and (99.5%, 50 mL) of ethyl acetate was used to extract it for three times to make a pale yellow oil, and then the organic layer was washed with KCl soln. and distilled water. After that, Na_2SO_4 was used to dry and filter it; the solvent was evaporated under a low pressure. Chromatography was done in a flash (9:1 silica gel, n-hexane: ethyl acetate) Rf = 0.75 for [BPMP] in bright yellow liquid (2.23 g, percent) (9:1 n-Hexane: ethyl acetate).

C-Synthesis of 2,6-bis(((1-octyl-1H-1,2,3-triazol-4-yl) methoxy) methyl) pyridine [BOTMMP/L]

[BPMP] (99%, 0.215 g, 1 mmol) was added dropwise to (3) mL of DMSO to a heterogeneous mixture of (98%, 0.039 g, 0.2 mmol) of sodium ascorbate and (0.025 g, 0.01 mmol) of $CuSO_4.5H_2O$ in (2) mL of DMSO. After stirring for 2 minutes, 1-azidooctane was added to the mixture (3 mmol). The mixture was stirred and heated for 48 hours at (50-60) °C. (30) mL of distilled water was added to dilute it, and then it was extracted three times by DCM (99%, 50 mL), dehydrated by using Na_2SO_4, and evaporated under low pressure. After flash chromatography, the Rf value is 0.17 (silica gel, 2 of EtOAc: 1 of n-Hexane). The final product has a white solid appearance (the desired chemical is obtained).

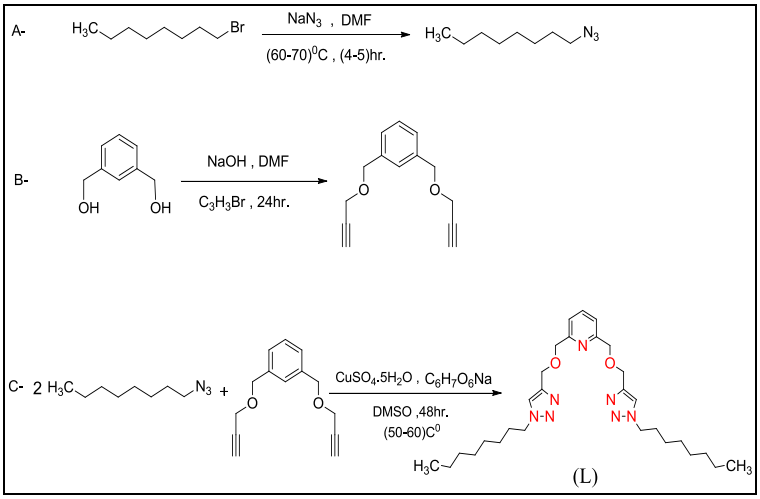

SCHEME 2 Steps of synthesis of the ligand [BOTMMP/L]

Metal-complexation [13]

Each metal salt is in an ethanoic solution, where the reaction occurs (1mmol) [$MnCl_2$ (98%, 0.161g), $PdCl_2$ (98%, 0.177g), and $HAuCl_4.H_2O$ (51%, 0.411g)] were added to (10 mL) of ethanoic solution to (0.525g, 1mmol) of ligand with stirring in a (1:1) molar ratio. For 2–3 hours, it was refluxed with heating the

mixture of reaction to produce a colored precipitate, they were filtered, repeatedly rinsed with ether, and then desiccated dried before. The spectroscopic, analytical, and physical measures were used to identify each generated complex, as indicated in Table 1.

The synthesized metal complexes' and its ligand bioactivity

A disc diffusion method [14] was used in this study to examine the behavior of the ligand (L) that was produced and its metal complexes as antimicrobial (against *Staphy. aureus*, and *E. coli*) and (against *cand. albicaus*). Tested micro-organisms were cultured in nutrient agar medium. The samples of compounds freshly prepared in three concentrations (10, 50, and 200) ppm by dissolving in dimethyl sulfoxide. Then, the plates were incubated in 37 °C for one day (24 hours), and the inhibition zone of micro-organisms growth around the disc checked. The antimicrobial test was repeated twice for each concentration within 24 hours. Table 4 depicts the results of bioactivity assay.

Results and discussion

The resulting complexes and their chelated were colored powders that remained stable in the open atmosphere for a long period. Table 1 lists the physio-chemical properties of the resulting compounds. The results of the metal analysis are in a good agreement with the calculated values in a satisfactory manner. Measurements of spectral and magnetic moments backed up the proposed molecular formula.

TABLE 1 Summary of physical and analytical data for synthesized substances

Compounds	Color	Molecular weight g/mol	Melting point (°C)	Yield %	Elemental analysis Found (calc.)			Metal % found (calc.)	Suggested Molecular formula
					C	H	N		
L	White	525.73	85-87	72.11	65.80 (66.20)	8.45 (9.01)	18.11 (18.65)	–	$C_{29}H_{47}N_7O_2$
L-Mn^{2+}	Light pink	669.60	169-171	71.6	51.74 (52.02)	7.17 (7.38)	14.35 (14.64)	7.95 (8.20)	$C_{29}H_{49}Cl_2N_7O_3Mn$
L-Pd^{2+}	brown	703.06	245-247	77.14	49.16 (49.49)	6.32 (6.68)	13.45 (13.94)	14.89 (15.14)	$C_{29}H_{47}Cl_2N_7O_2Pd$
L-Au^{3+}	Orang	829.06	170-172	95.7	42.27 (42.75)	5.34 (5.71)	11.29 (11.82)	23.18 (23.76)	$C_{29}H_{47}Cl_3N_7O_2Au$

Infrared spectroscopic study

A study of Infrared spectroscopy with CsI disc was used to record all of the spectra in the solid-state. As expected, FT.IR provided useful information on the ligand [L] behavior with various metal ions based on a comparison with published data [15]. Octyl bromide and sodium azide undergo an SN_2 reaction in DMF was used to make the compound 1-azidooctane. The extremely distinctive absorption of azide group at 2094 cm^{-1} which is depicted in the FT-IR spectra of 1-azidooctane, Figure 1, is strong evidence for the synthesis of the compound 1-azidooctane [16]. Figure 2 displays the FT-IR spectra of the compound [BPMP]. The reaction was effective, as evidenced by the evanescence of a broad band at (3354) cm^{-1} and the occurrence of sharp bands in the regions (3308 and 2121) cm^{-1} attributable to the groups υ (C–H and C≡C) of the terminal alkyne, respectively, in the FT-IR spectra [17]. In addition, the spectrum of the ligand revealed in Figure 3 provides strong evidence that cycloaddition reaction was successful, with bands disappearing around (2094, 2117) cm^{-1}, demonstrating the formation of the aromatic triazole ring and weak bands appearing at (3091, 1653) cm^{-1}, indicating that cycloaddition reaction was successful [18].

The observed bands of the free ligand L spectrum which are located in the regions

(3091, 3136, 1595, 1508, 1220, and 1122) cm^{-1} that attributed to the frequencies $\upsilon(C\text{-}H)_{Pyridine}$, $\upsilon(C\text{-}H)_{Triazole}$, $\upsilon(N{=}N)_{Triazole}$, $\upsilon(C{=}N)_{Pyridine}$, $\upsilon(C\text{-}N)_{Triazole}$, and $\upsilon(C\text{-}O\text{-}C)_{Ether}$, respectively [19].

In the complexes, the frequency of υ (N=N) moved to increased frequency at about (4-11) cm^{-1}, while υ (C-N)Triazole, υ (C=N)Pyridine, and υ (C-O-C)Ether frequencies changed to higher frequencies at roughly (6-18), (1-51) cm^{-1}, and (31-35) cm^{-1}, respectively [20]. The complexes of (L-Mn) exhibit novel bands for υ (Mn-N)pyridine at (271) cm^{-1} and υ (M-O) at (435-464) cm^{-1} and $\upsilon(M\text{-}N)_{triazole}$ that appear at (503-532) cm^{-1} in the complexes spectra. Other bundles are indicated in Table 2 besides υ (Mn-Cl), which appears at (324) cm^{-1}[21]. As a result, we have suggested that in the solid state, the complexes display four and six coordination geometries. Figures (1-6) display the FT-IR spectrum.

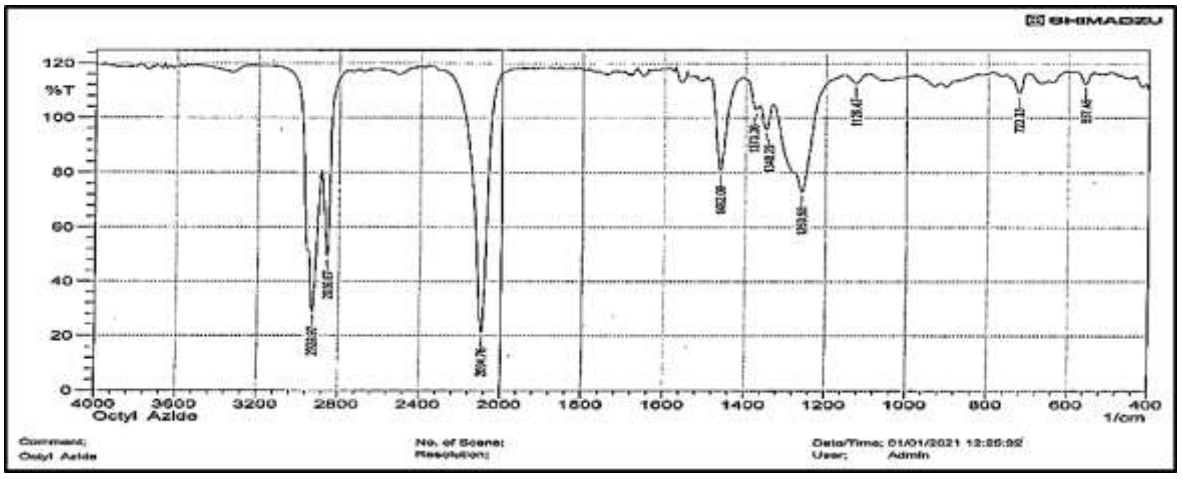

FIGURE 1 The FT-IR spectrum of 1-azidooctane compound

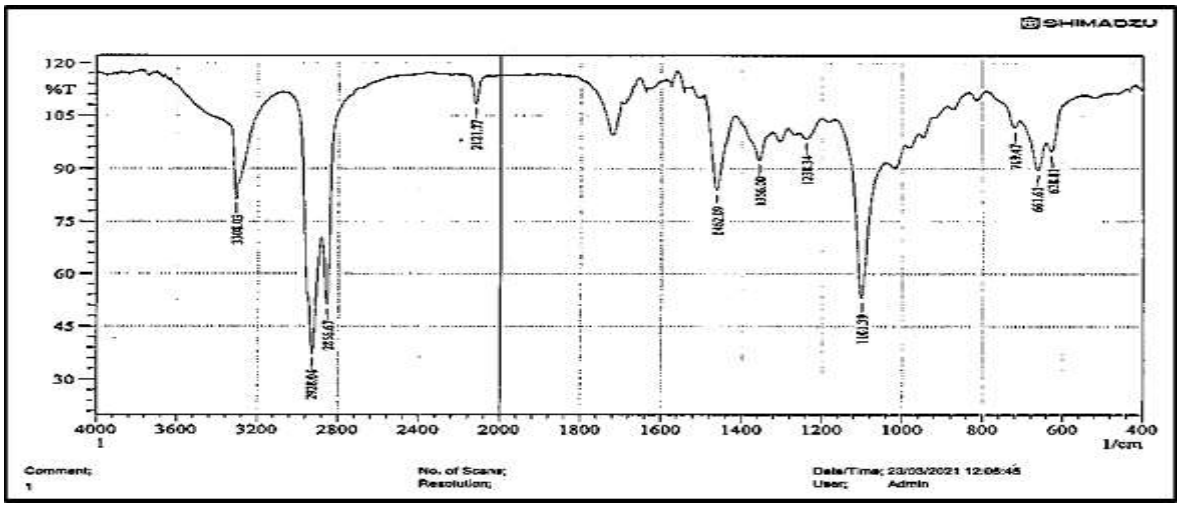

FIGURE 2 The FT-IR spectrum of [BPMP] compound

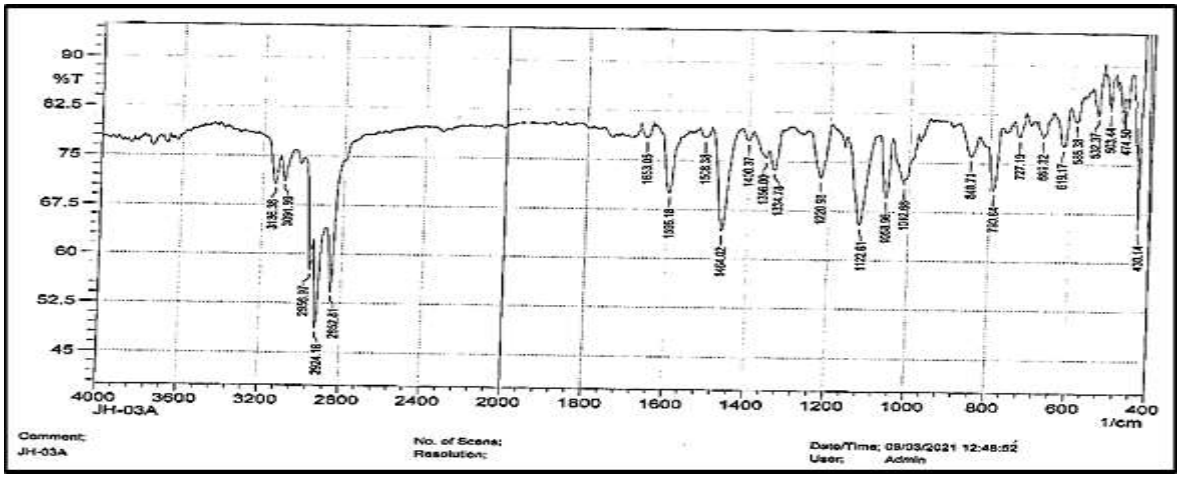

FIGURE 3 The FT-IR spectrum of [L] compound

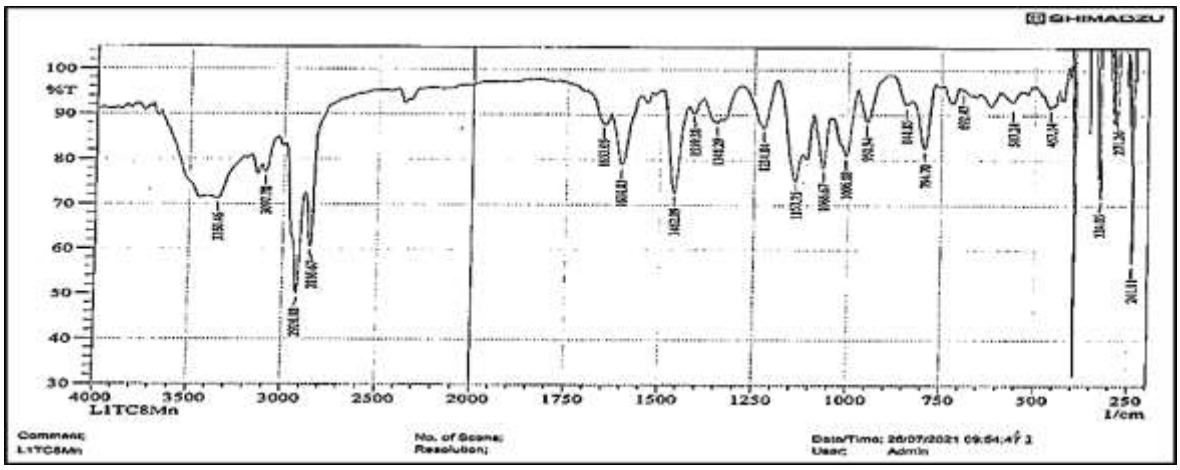

FIGURE 4 The FT-IR spectrum of prepared complex of Mn(II)

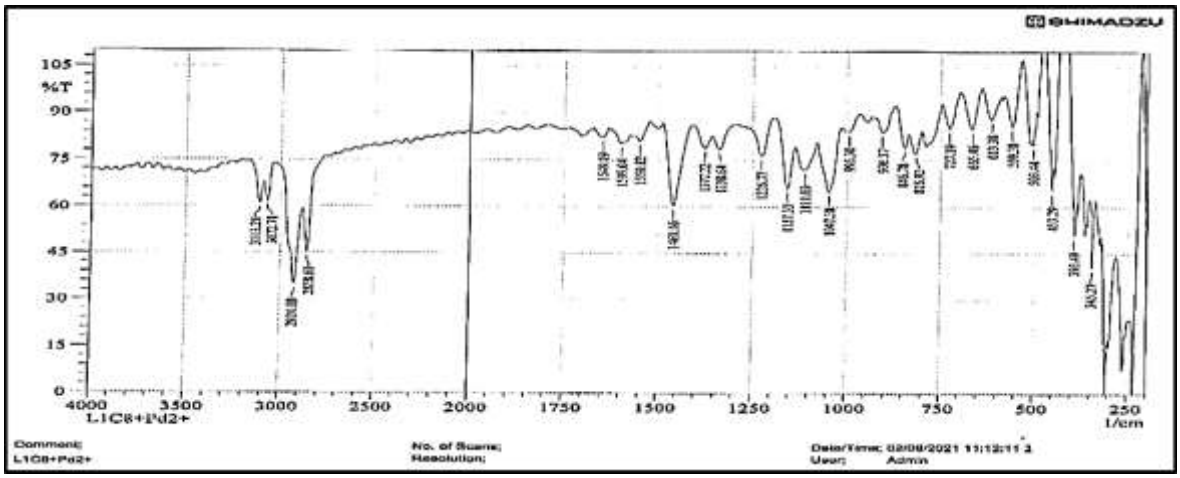

FIGURE 5 The FT-IR spectrum of prepared complex of Pd(II)

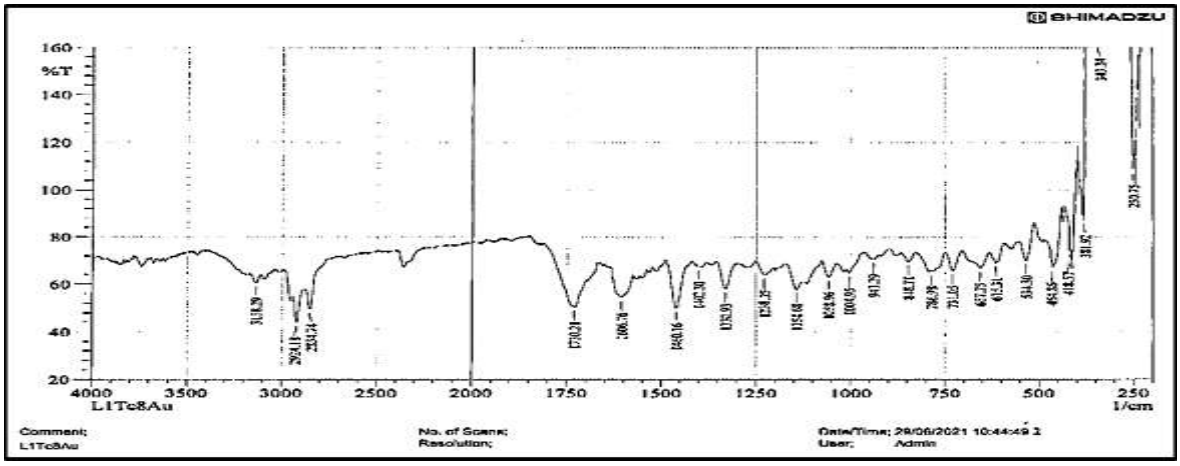

FIGURE 6 The FT-IR spectrum of prepared complex of Au(III)

TABLE 2 Selected bands of FT-IR spectra of the prepared compounds in cm^{-1}

Compound	υ(N=N) tri.	υ(C=N) py.	υ(C-N)tri	υ(C-O-C)ether	υ (M-N)py	υ(M-O)	υ(M-N) tri.	υ(M-Cl)
L	1595	1508	1220	1122	-	-	-	-
LMn	1604	1559	1234	1153	271	457	517	324
LPd	1599	1510	1226	1157	-	453	503	-
LAu	1606	1509	1238	1154	-	464	534	-

Measurements of conductivity, magnetic susceptibility, and electronic spectra

To verify the geometry of the produced complexes, additional structural tools were used, from the data of electronic spectra, magnetic moment, and electrical measurements. For their solution in DMSO, the UV-Vis. spectra of the complexes of (manganese, palladium, and gold) ions were obtained in the range (190-1100) nm.

A-Spectrum of [L]

Figure 7 displays the UV-Vis spectra of ligand (L), which shows three bands in the ultraviolet range. An inter ligand transition to (π→π*) on the pi-system caused the first band to arise at 42194 cm^{-1}. The second band of absorption, at 39062 cm^{-1}, was the same as the one which was derived from the (π→π*) transition, though it was belonged to a different group [22]. The appearance of the third absorption band at 37735 cm^{-1}, was linked to the (n → π*) electronic transition location on the oxygen and nitrogen atoms [23].

B-Spectrum of the Mn(II) complex

Light pink Mn(II) complex UV-Vis spectrum. Figure 8 demonstrate bands at (11235 and 26595) cm^{-1}, which back to the transitions $^6A_1g \rightarrow {}^4T_1g(G)$ (ν_1) and $^6A_1g \rightarrow {}^4A_2g + {}^4Eg(G)$ (ν_3) transitions, respectively, confirming previous research [24]. All the parameters (10Dq, B′, the value of the band of ν_2 assigned to the $^6A_1g \rightarrow {}^4T_2g(G)$ transition, and the nepelauxetic factor) were estimated according to the diagram of Tanaba-Sugano by fitting the ν_3/ν_1 ratio on the diagram of the octahedral d^5 structure. The ν_3/ν_1 =2.4 ratio fits the diagram at 1.53 Dq/B′, and the Racah parameter B' will be 714 cm^{-1} and β =0.83 (taking B^o of free ion to 860 cm^{-1}). The constant field splitting 10Dq value is 10924 cm^{-1}, which is nearly equivalent to the first transition. The magnetic value of 5.52 B.M. is observed, and when compared with other reporters [25], this degree is associated with the Mn (II) ion's octahedral geometry. This chemical is ionic based on its conductivity in DMSO at room temperature. The octahedral geometry around the Mn (II)

ion can be hypothesized by using data from analysis and spectroscopy, as depicted in Table 3.

C-Spectrum of the Pd(II) complex:

Two bands can be seen in the UV-Vis spectrum of Brown Pd(II) complex. The shoulder was the first absorption band to appear at 29411 cm^{-1}, followed by the more intense bands at 36764 cm^{-1}, as illustrated in Figure 9. For spin-parried d^8 square planer arrangement, these absorption bands were assigned to transition $^1A_1g \rightarrow {}^1B_1g$, which was represented to 10 Dq, and other $^1A_1g \rightarrow {}^1Eg$, respectively [26]. This assignment was based on the knowledge of palladium complexes with square planer shape, and it was matched with published data [27]. Magnetic susceptibility measurements revealed more evidence of square planer stereochemistry, confirming the low spin diamagnetic complex's evaluations [28]. The conductivity measurements revealed that this compound is an electrolyte. The structure of this complex can be postulated as square planer geometry based on the foregoing results and the IR spectra, which provided good support, as indicated in Table 3.

D-Spectrum of the Au(III) complex

The spectrum of the orang Au(III) ion has been identified by using the charge transfer bands that predominate the ligand field transitions. This implies that while the ligand field transition will be seen at a shorter wavelength, charge transfer bands will be visible at a greater wavelength [29]. We found two prominent bands at 27027 and 34482 cm^{-1} in the complicated gold spectra depicted in Figure 10, which are $^1A_1g \rightarrow {}^1B_1g$, $^1A_1g \rightarrow {}^1Eg$ transitions, respectively, and the other peak appeared at 37037 cm^{-1} attributed to charge transfer in a square planer geometry [30]. The magnetic moment is zero, as listed in Table 3. This chemical is ionic based on its conductivity in DMSO at room temperature. Based on data analysis and spectroscopy methods, a square planer structure for this molecule can be predicted.

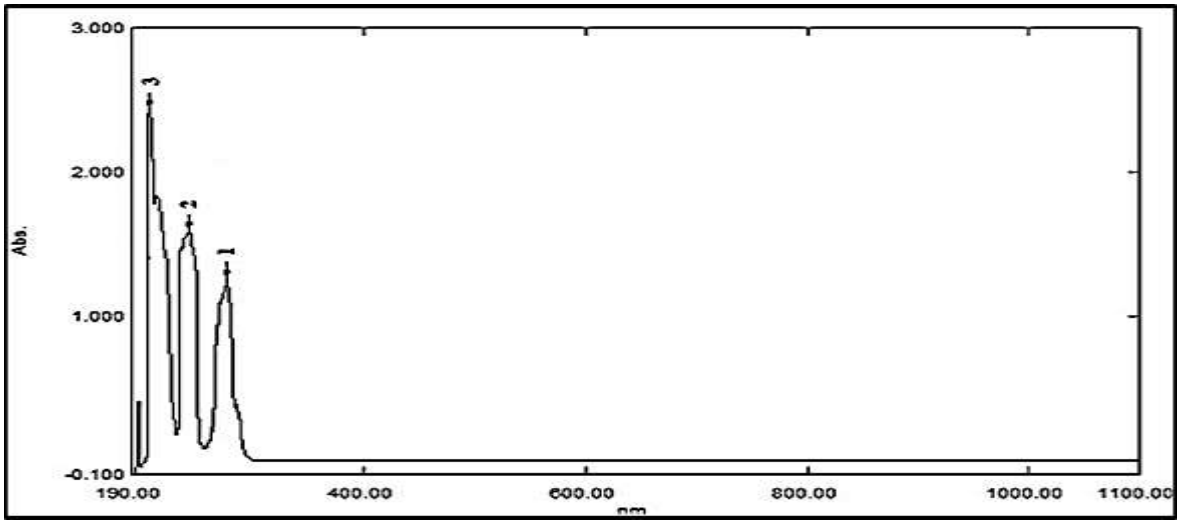

FIGURE 7 The electronic spectrum of the ligand

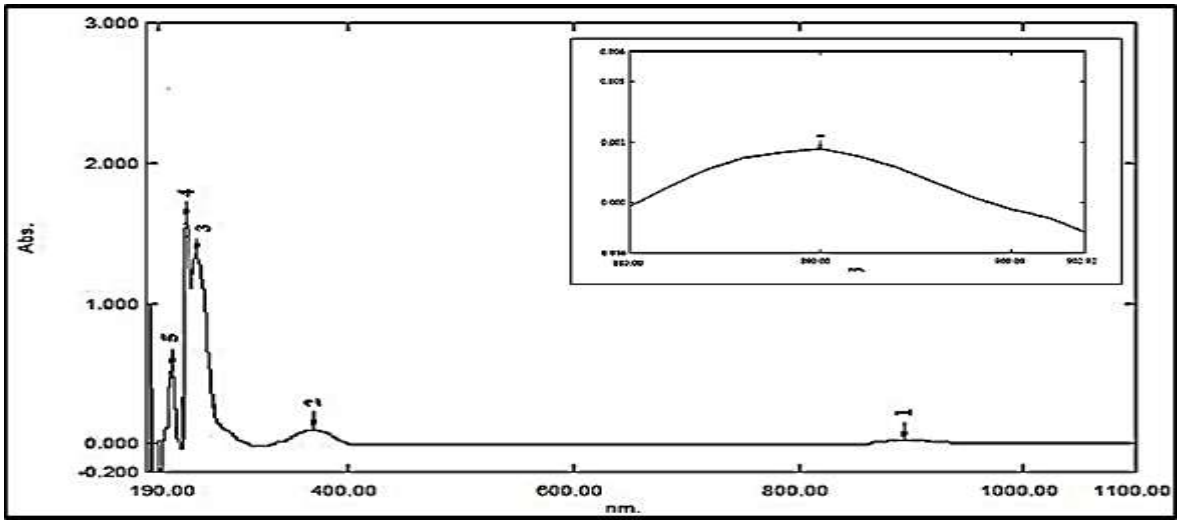

FIGURE 8 The electronic spectrum L-Mn(II) complex

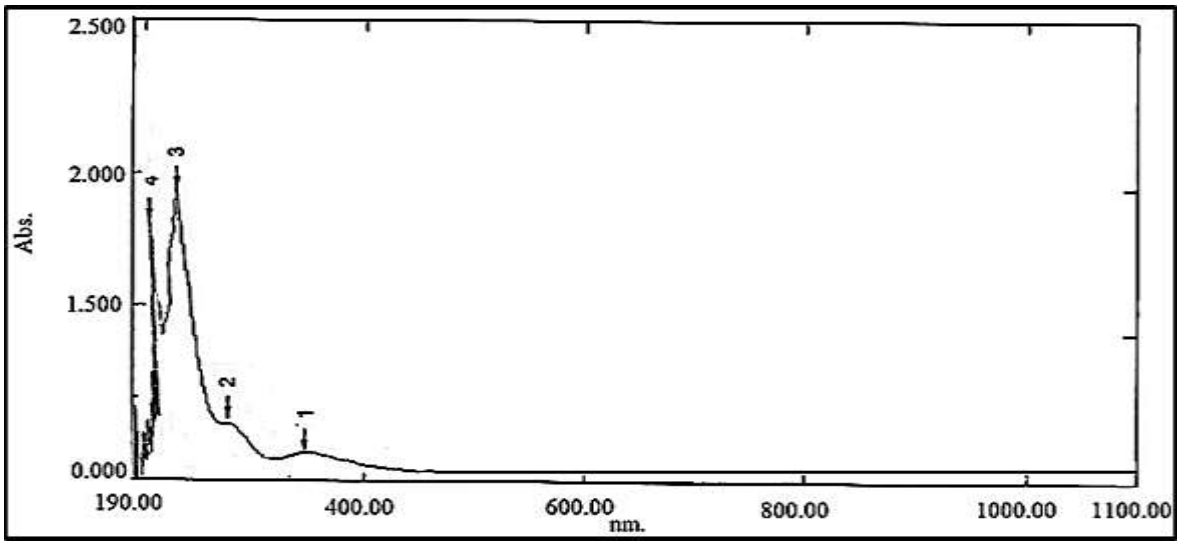

FIGURE 9 The electronic spectrum L-Pd(II) complex

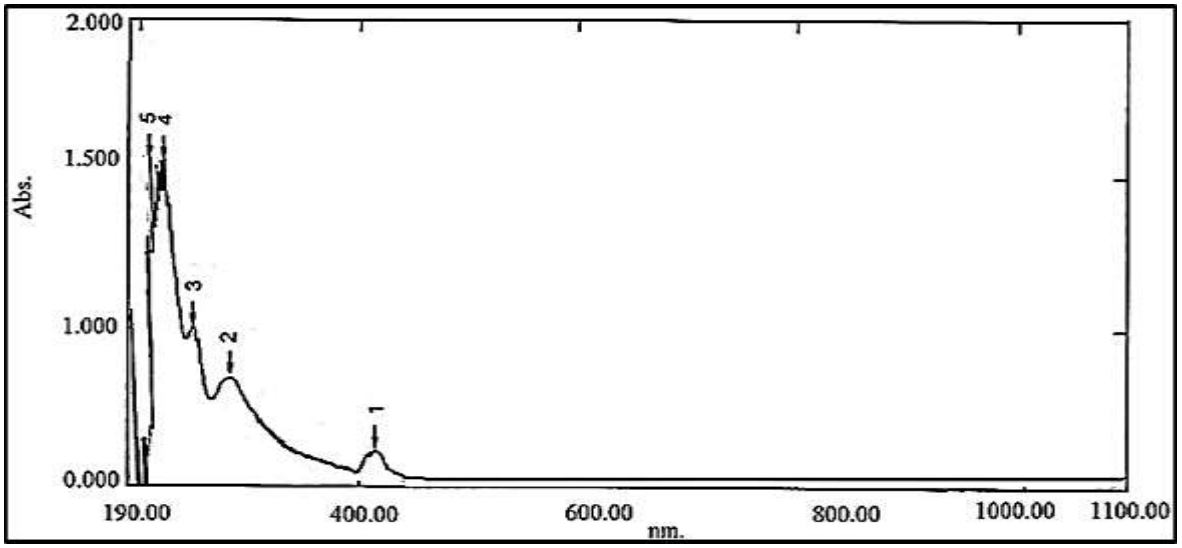

FIGURE 10 The electronic spectrum L-Au(III) complex

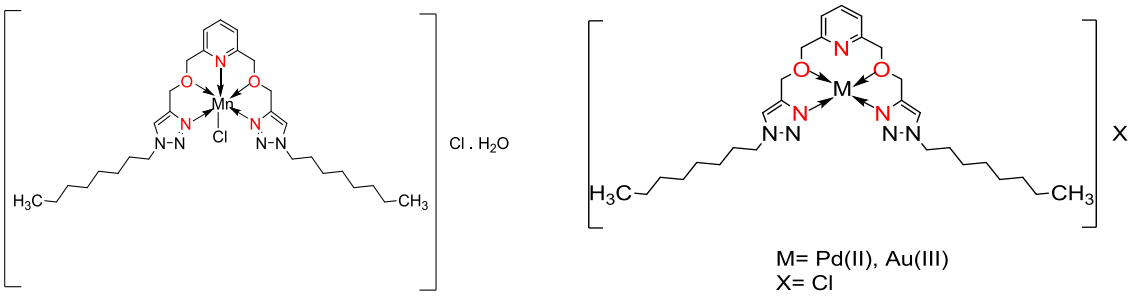

SCHEME 3 Proposed geometry of synthesized complexes

TABLE 3 In a DMSO solvent, complex structural insights, electronic spectroscopy data, conductivity tests, and magnetic moments

Component	Abs. cm^{-1}	Assignments	μeff B.M	μs. cm^{-1}	Suggested geometry
L	37735 39062 42194	$n \rightarrow \pi^*$ $\pi \rightarrow \pi^*$	-	-	-
L-Mn	11235 17820 26595	$^6A_1g \rightarrow {}^4T_1g_{(G)}$ $^6A_1g \rightarrow {}^4T_2g_{(G)}$ $^6A_1g \rightarrow {}^4A_2g + {}^4Eg_{(G)}$	5.52	38.2	Octahedral
L-Pd	29411 36764	$^1A_1g \rightarrow {}^1B_1g$ $^1A_1g \rightarrow {}^1Eg$	0.00	80.5	Square planer
L-Au	27027 34482 37037	$^1A_1g \rightarrow {}^1B_1g$ $^1A_1g \rightarrow {}^1Eg$ Au →LCT	0.00	297.3	Square planer

NMR spectra of [L] and it complexes

^{1}H-NMR spectrum

Figure 11 reveals the ^{1}H-NMR spectra of the ligand [L] in DMSO-d^6 solvent. Many peaks exist at the range (1.89-1.20) ppm (d,2H, H_2-H_7 and H_{23}-H_{28}), which emerge at the range (7.68-7.26) ppm of which several peaks are caused by the protons of (CH_2) aliphatic series groups, (t, H, H_{14}-H_{16}) and (s,H_9,H_{21}), and the pyridine (CH) groups and protons from triazole rings [31], respectively, as well as a peak that emerged in the (4.67-4.74) ppm range (d,2H, H_8, H_{12}, H_{18}, and H_{22}). CH_2 the aliphatic chain's initial group is attached to the triazole ring, while the CH_2 group is linked to the pyridine ring. Signal is also depicted as peaks in ppm (4.32-4.30) (s, 2H, H_{11}, and H_{19}) [32]. The comparison of ^{1}HNMR spectra for Mn(II) and Au(III) complexes produced with the proton's position in the ligand spectrum indicated the coordination, with these metal complexes, the ligand's proton position barely shifts. At about (2.5) ppm, the DMSO displays a singlet peak, as illustrated in Figures 12 and 13.

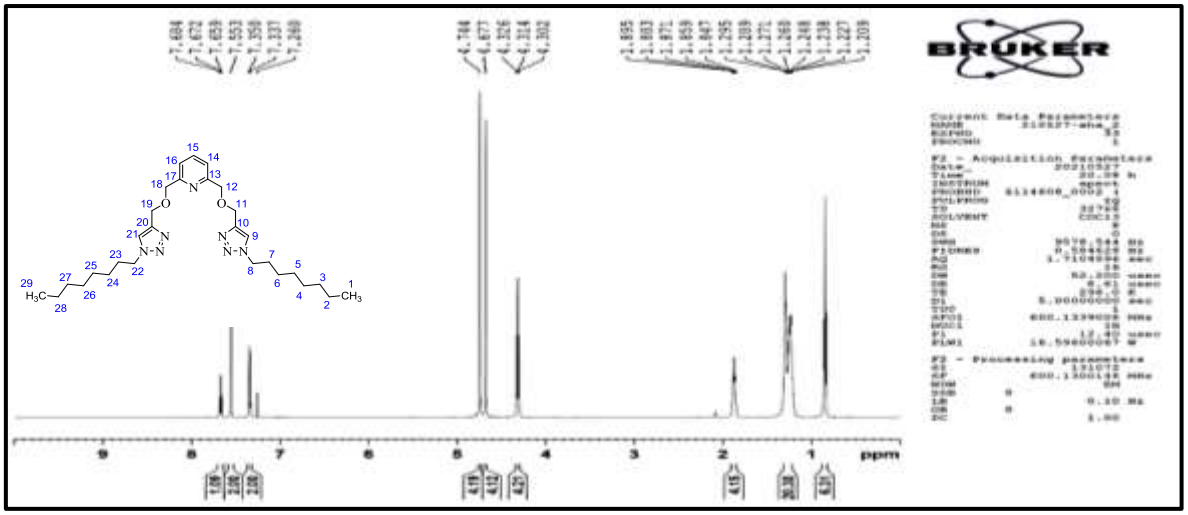

FIGURE 11 Spectrum of ^{1}H-NMR of [L]

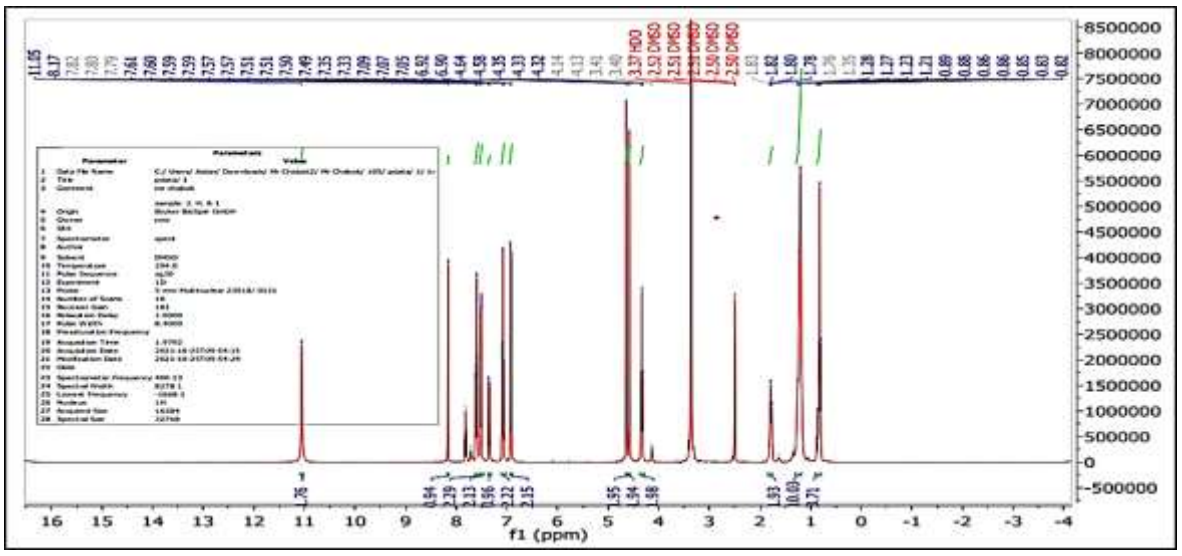

FIGURE 12 Spectrum of ^{1}H-NMR of L-Au$^{(III)}$

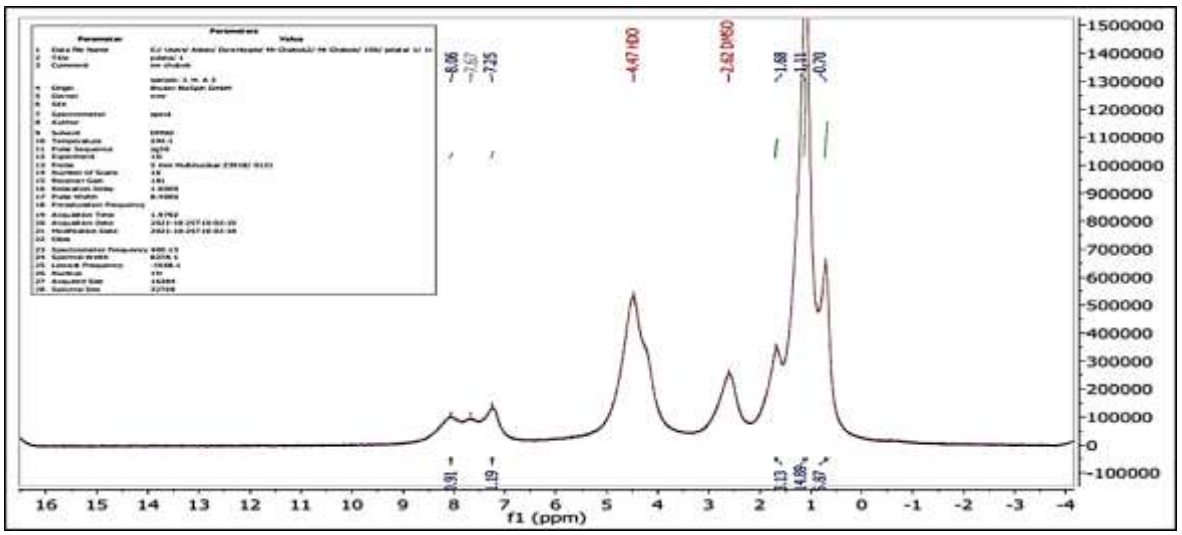

FIGURE 13 Spectrum of ^{1}H-NMR of L-Mn$^{(II)}$

^{13}C-NMR spectrum

Figure 14 displays the ligand [L]^{13}C-NMR spectra in DMSO-d^{6} solvent many peaks between (31.7-22.6) ppm (s, C, C_2-C_7, and C_{23}-C_{28}) ppm which groups in the aliphatic sequence return to carbon. The CH_3 terminal group, however, only displayed one peak at (14.1) ppm (s, C, and C_1-C_{29}). However, the triazole ring's initial aliphatic chain, CH_2, produced a single peak at (50.4) ppm (s, C, C_8, and C_{22}) [33]. On the other hand, the CH_2 group connected to the triazole ring displayed a single peak at (64.4) ppm (s, C, C_{11}, and C_{19}). In the case of (CH_2) linked to the pyridine ring, the range (77.3-73.3) ppm showed a peak (s, C, C_{12}, and C_{18}). In addition, the triazole ring and $(CH)_{group}$ of the pyridine showed peak at δ (120.4, 122.4) pmm (s, C, C_{14}, and C_{16}) and it displayed peak at δ (137.4, 144.8, and 157.5) (s, C, C_{15}, C_{10}, C_{20}, C_{13}, and C_{17}), respectively [34,35]. The ^{13}CNMR spectra of the Au (III) complex produced were compared with the ligand spectrum. One peak has replaced the former peak of CH_2, the first group in the aliphatic chain attached to the triazole ring at (49.7) ppm (s, C, C_8, and C_{22}). On the other hand, the CH_2 group connected to the triazole ring revealed one peak at (63.9) ppm (s, C, C_{11}, and C_{19}). As for (CH_2) pertaining to the pyridine ring revealed peak at δ (72.6) ppm (s, C, C_{12}, and C_{18}). Besides, the triazole ring and (CH) group of the pyridine revealed a peak in the range δ (125.1, 112.6) ppm (s, C, C_{14}, and C_{16}) and the showed peake at δ (138.8, 151.1, and 159.8) (s, C, C_{15}, C_{10}, C_{20}, C_{13}, and C_{17}), respectively. The coordination compounds are confirmed by the groups in the ligands of these metal complexes, as displayed in Figures 15-17.

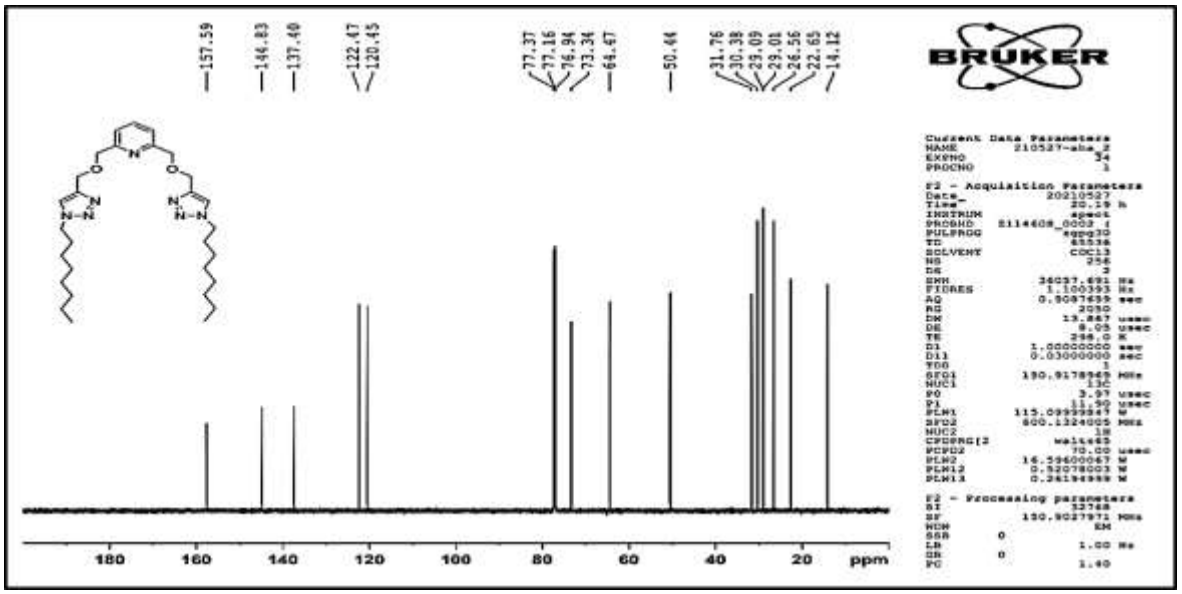

FIGURE 14 Spectrum of ^{13}C-NMR of [L]

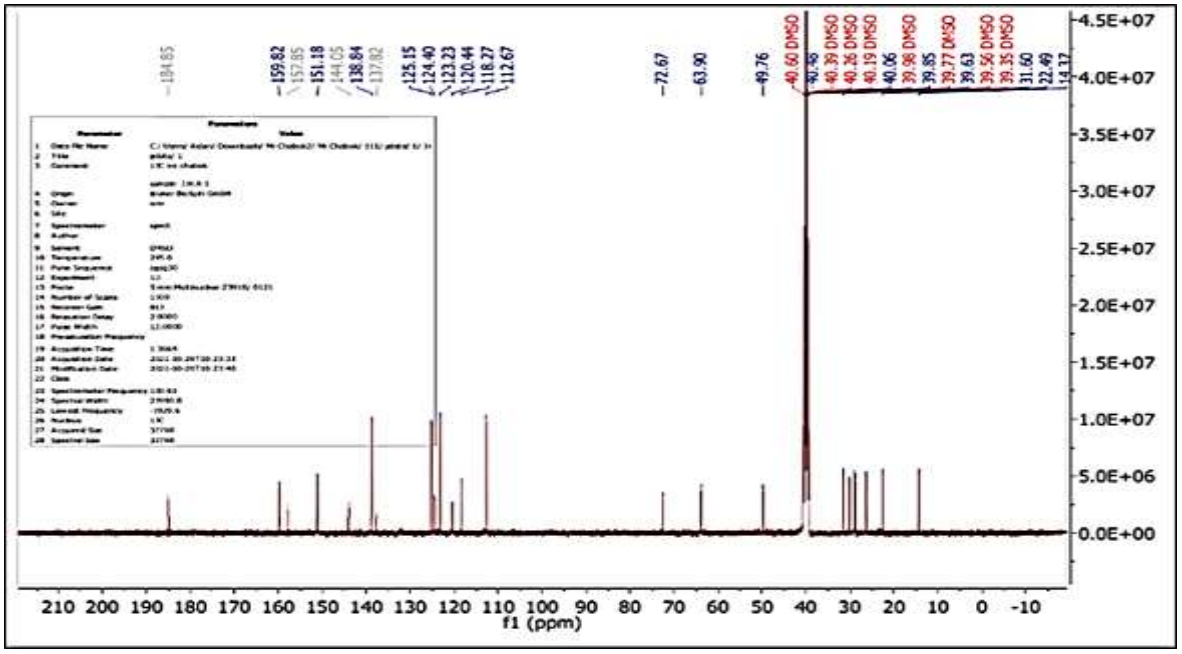

FIGURE 15 Spectrum of ^{13}C-NMR of L-Au$^{(III)}$

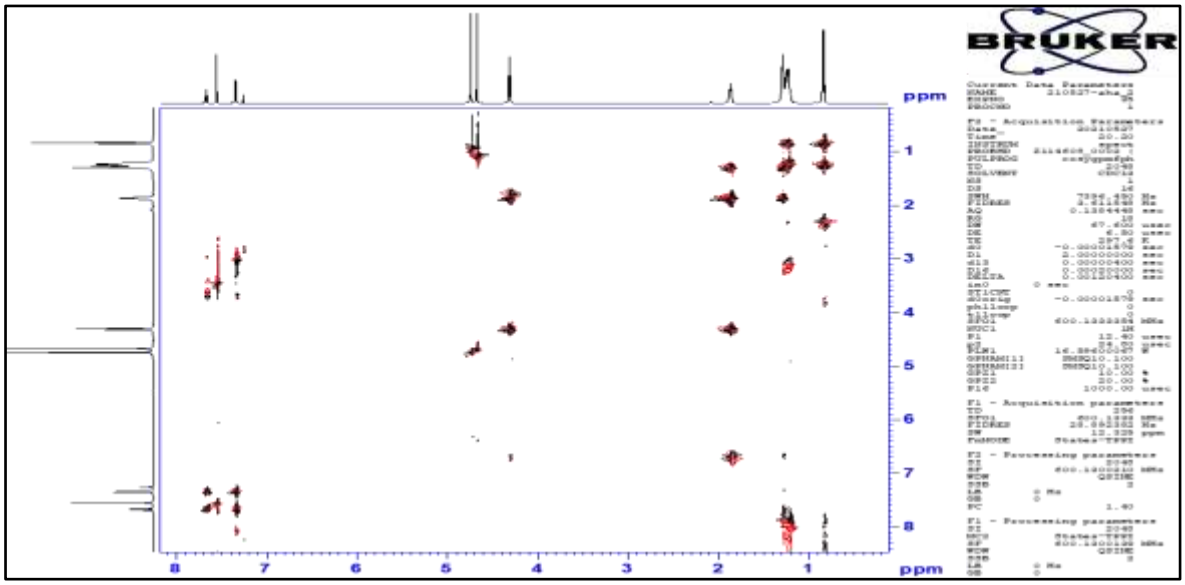

FIGURE 16 [L] COSY spectrum

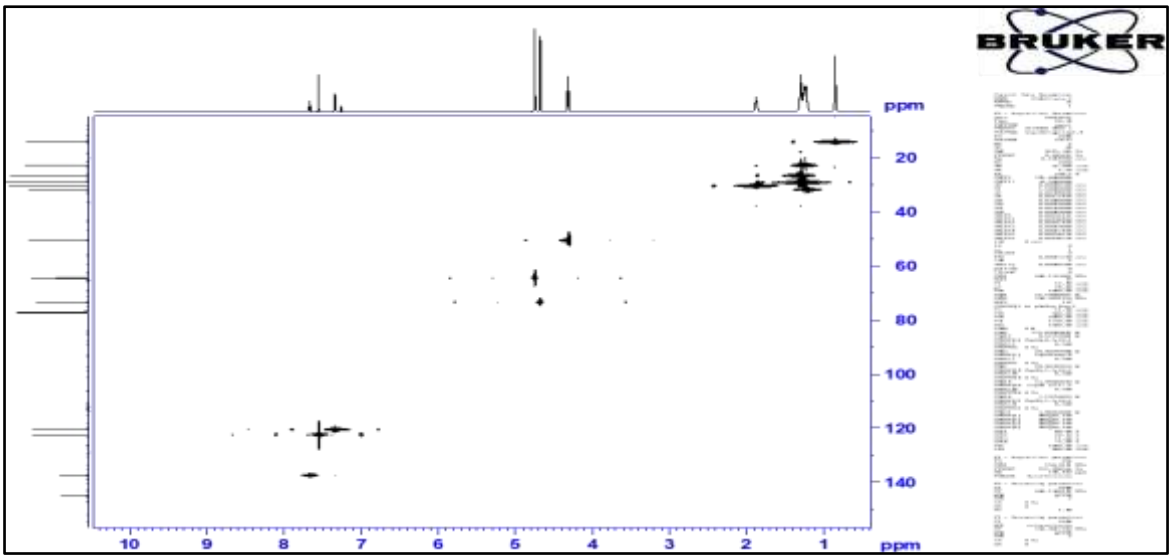

FIGURE 17 [L] HSQC spectrum

Mass spectra

Ligand mass spectra

From analyzing the mass spectra of the ligand [L], that shown in Figure 18, many triazole derivatives with various substituents have been proposed and studied. The development of a base peak at mz^{+}=548.368 $g.mol^{-1}$ that corresponds to the formula $[M + Na]^{+}$ in HRMS, which aligned well with the experimental ligand formula ($C_{29}H_{47}N_7O_2$+Na), confirms the ligand production.

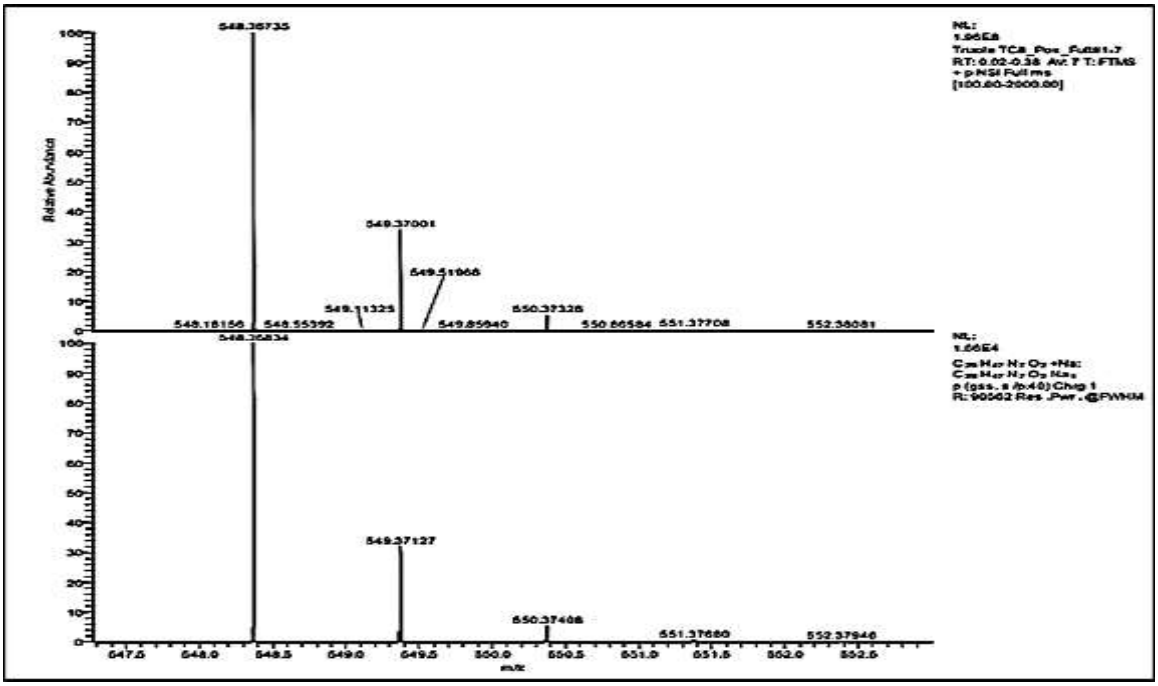

FIGURE 18 Mass spectrum of [L]

L-Au(III) complex mass spectra

The obtained fragmentation for the complex is indicated in Figure 19 and the proposed formula matches the molecular weight. The emergence of a base peak at mz^{+}=828.6 $gmol^{-1}$, which corresponds to the formula $C_{29}H_{47}Cl_3N_7O_2Au$ and is in good agreement with the experimental L-Au(III) formula, serves as confirmation of the creation of the complex.

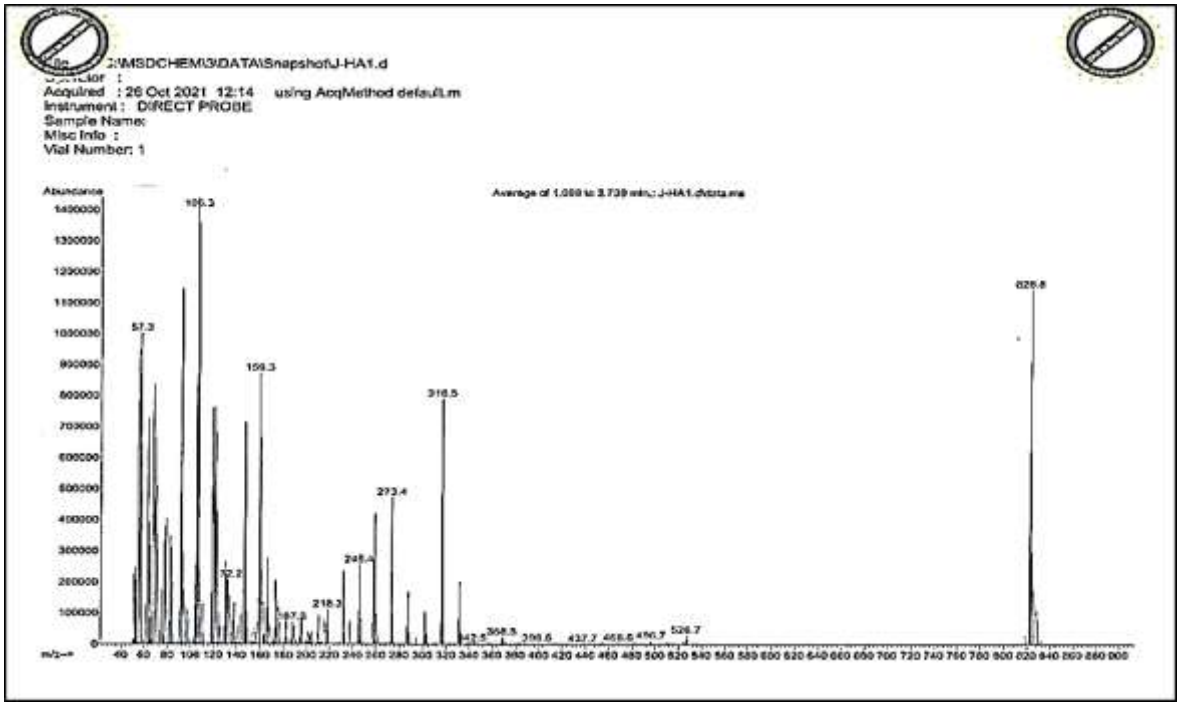

FIGURE 19 Mass spectrum of L-Au(III) complex

Biological activities

As a practical application for prepared complexes and their ligand, the biological activity of these compounds was estimated. The activities evaluations were screened in vitro against *Staphy. aureus* as a gram-positive and *E. coli* as a gram-negative species, in addition to antifungal activity against the micro-organism *cand. albicaus*, employing three distinct (10, 50, and 200 ppm) concentrations of each chemical.

The findings demonstrate that, at greater concentrations, the majority of complexes are more hazardous to these bacterial and fungal species than the free ligand. Likewise, we can note that the complexes and their ligand have indicated a higher resistance behavior towards a gram-negative species (Escherichia coli) compared with their activity with other micro-organisms.

The activity of metal ion complexes, Figure 20, may be due to the impact of metal ions on the normal cell membrane [36,37]. The polar and non-polar characteristics of metal chelates are combined, as it is well-known; this gives them the ability to penetrate the cell wall easily. In addition, the Tweedy's chelation idea may be used to explain this elevated activity [38]. Furthermore, the thought to be hard metal ions make their complexes less lipophilic, which comparatively slows their penetration through the lipid component of the cell membrane. This is an example of the synergistic effect of the metal ion and organic molecule. In contrast, salt metal ions make their complexes more lipophilic, which make it easier for them to penetrate cell walls and change the environment of the cells.

In addition to the above points, the behavior of the compounds towards the examined micro-organisms can be attributed to the factors such as: metal ion nature, the geometrical structure of these complexes, the arrangement of the ligands around the metal ion, the chelation effect of the organic molecules utilized as ligands, the nature of the atoms that coordinate with metals, and the type and oxidation state of the metals.

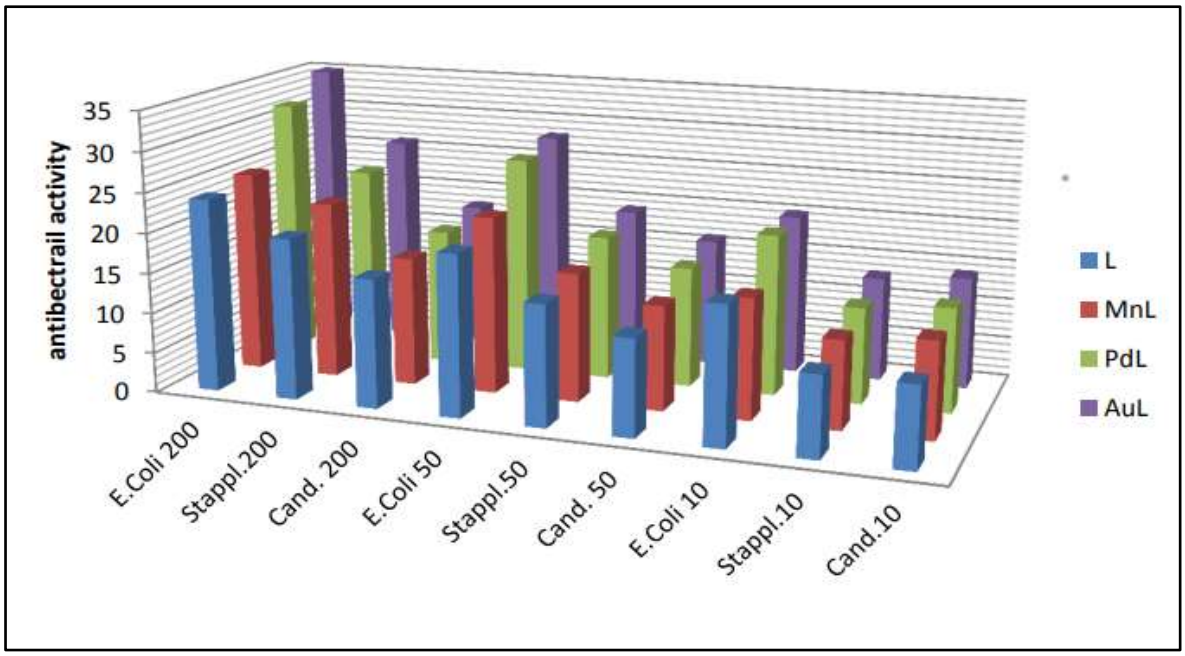

FIGURE 20 Biological activity of prepared compounds

TABLE 4 The widths of inhibition zone caused by the ligand's antibacterial and antifungal action are shown by its metal complex (mm)

Component	*Escherichia coli* *E.coli*			*Staphylococcus aureus* *Staphy.*			*Candida albicans* *Cond.*		
	200 ppm	50 ppm	10 ppm	200 ppm	50 ppm	10 ppm	200 ppm	50 ppm	10 ppm
L	24	20	17	20	15	10	16	12	10
L-Mn(II)	25	22	15	22	16	11	16	13	12
L-Pd(II)	32	27	20	24	18	12	17	15	13
L-Au(III)	35	28	20	26	19	13	18	16	14

Conclusion

The data from the spectral and physical analysis indicated that the preparation of 2,6-bis(((1-octyl-1H-1,2,3-triazol-4-yl) methoxy) methyl) pyridine from starting materials was success, also the process of complexes formation using 1,2,3-triazol derivative as ligand with some light and heavy metals (Mn^{2+}, Pd^{2+} and Au^{3+}) was done with the molar ratio 1:1 of metal to ligand, where the ligand behave as tetra and penta-dentate through O and N atoms. All synthesized complexes have ability to electrical conductivity and the suggested geometries were octahedral for Mn-complex and square planer for Pd, Au – complexes.

The organic ligand and their complexes were applied as antimicrobial in vitro against *Staphy. aureus* as a gram-positive and *E. coli* as a gram-negative species, in addition to antifungal activity against the micro-organism *cand. albicaus*, employing three distinct (10, 50, and 200 ppm) concentrations of each chemical. The results indicate that synthesized complexes are more active than their ligand and the activity enhanced with increasing concentration. The compounds behave as strong growth inhibition ability towards *Escherichia coli.* as compared with other tested micro-organism. In general, the overall order of efficiency of prepared compounds was as follow: Au-L > Pd-L > Mn-L > L.

Acknowledgements

I would like to express my deep gratitude and appreciation to my lovely supervisor professor Dr. Mohsin E. Aldokheily for his guidance, suggestions, support, and encouragement through the research period. Also, I would like to extend my sincere thanks to my supervisor, Dr. Athraa Hameed, for the assistance and support during the study period.

Orcid:

Jihan Hameed Abdulameer:
https://www.orcid.org/0000-0003-2850-8458

References

[1] E. Güzel, *RSC Adv*., **2019**, *9*, 10854–10864. [Crossref], [Google Scholar], [Publisher]
[2] P.L. Carver, *Met. Ions Life Sci*., **2019**, *19*, 1-16. [Crossref], [Google Scholar], [Publisher]
[3] K. Indira, U.K. Mudali, T. Nishimura, N. Rajendran, *J. Bio- Tribo-Corrosion*, **2015**, 1. [Crossref], [Google Scholar], [Publisher]
[4] N. Gümrükçüoğlu, Z. Bahadır, M. Ocak, and Ü. Ocak, *Pak. J. Anal. Environ. Chem*., **2013**, *14*, 58–64. [Google Scholar], [Publisher]
[5] A. Noor, J.E.M. Lewis, S.A. Cameron, S.C. Moratti, J.D. Crowley, *Supramol. Chem*., **2012**, *24*, 492–498. [Crossref], [Google Scholar], [Publisher]
[6] T.D. Nandgude, J.N. Jadhavrao, A.R. Jawlekar, S.S. Poddar., *Pharmaceutical Resonance*., **2020**, *2*, 47–54. [Crossref], [Google Scholar], [Publisher]
[7] M.T. Alsaba, M.F. Al Dushaishi, A.K. Abbas, *J. Pet. Explor. Prod. Technol*., 2020, 10, 1389–1399. [Crossref], [Google Scholar], [Publisher]
[8] P.I.P. Elliott, *Organomet. Chem*., **2014**, *39*, 1–25. [Crossref], [Google Scholar], [Publisher]
[9] S.M. Emam, D.A. Tolan, A.M. El-Nahas, *Appl. Organomet. Chem*., **2020**, *34*, 1-26. [Crossref], [Google Scholar], [Publisher]
[10] N.S. Al-Radadi, E.M. Zayed, G.G. Mohamed, H.A. Abd El Salam, *J. Chem*., **2020**, *2020*, 1-12. [Crossref], [Google Scholar], [Publisher]
[11] M. Gaber, H.A. El-Ghamry, S.K. Fathalla, *Appl. Organomet. Chem*., **2020**, *34*, 1-12. [Crossref], [Google Scholar], [Publisher]
[12] D. Mondal, M.S. Balakrishna, *Eur. J. Inorg. Chem*., **2020**, *2020*, 2392-2402. [Crossref], [Google Scholar], [Publisher]
[13] J.H. Abud Almeer, M.F. Alias, *Chem. Methodol*, **2022**, *6*, 184-196. [Crossref], [Publisher]
[14] H. Hernández-López, S. Leyva-Ramos, C.F.A. Gómez-Durán, A. Pedraza-Alvarez, I.R. Rodríguez-Gutiérrez, M.A. Leyva-Peralta, R.S. Razo-Hernández., *ACS Omega*, **2020**, *5*, 14061–14068. [Crossref], [Google Scholar], [Publisher]
[15] R.S. Meinel, A.C. Almeida, P.H.F. Stroppa, N. Glanzmann, E.S. Coimbra, A.D. da Silva, *Chem. Biol. Interact*., **2020**, *315*, 108850. [Crossref], [Google Scholar], [Publisher]
[16] R. García-Monroy Davir González-Calderón, A. Ramírez-Villalva, S. Mastachi-Loza, J. G. Aguirre-de Paz, A. Fuentes-Benítes, C. González-Romero, *J. Mex. Chem. Soc*., **2021**, *65*, 202–213. [Crossref], [Google Scholar], [Publisher]
[17] S.E. Motika, X. Shi, *Arkivoc*, **2018**, *2018*, 280–287. [Crossref], [Google Scholar], [Publisher]
[18] S. Kaur, P. Kaur, *Indo Glob. J. Pharm. Sci*., **2019**, *09*, 146–146. [Crossref], [Google Scholar], [Publisher]
[19] M.N. Joy, Y.D. Bodke, S. Telkar, V.A. Bakulev, *J. Mex. Chem. Soc*., **2020**, *64*, 46–66. [Crossref], [Google Scholar], [Publisher]
[20] D.V. Francis, D.H. Miles, A.I. Mohammed, R.W. Read, X. Wang, *J. Fluor. Chem*., **2011**, *132*, 898–906. [Crossref], [Google Scholar], [Publisher].
[21] H.C. Kolb, M.G. Finn, K.B. Sharpless, *Angew. Chemie-Int. Ed*., **2001**, *40*, 2004–2021. [Crossref], [Google Scholar], [Publisher]
[22] N. Thondavada, R. Chokkareddy, G.G. Redhi, *Green Metal Nanoparticles*, **2018**, 603–627. [Crossref], [Google Scholar], [Publisher]
[23] N.S. Al-Radadi, E.M. Zayed, G.G. Mohamed, H.A. Abd El Salam, *J. Chem*., **2020**, *2020*. [Crossref], [Google Scholar], [Publisher]

[24] T. El Malah, H.F. Nour, A.A.E. Satti, B.A. Hemdan, W.A. El-Sayed, *Molecules*, **2020**, *25*, 1–17. [Crossref], [Google Scholar], [Publisher]
[25] M. Lungu, A. Neculae, M. Bunoiu, C. Biris, *Nanoparticles' Promises Risks Charact. Manip. Potential Hazards to Humanit. Environ.*, **2015**, 1–355. [Crossref], [Google Scholar], [Publisher]
[26] E.C. Koch, *Propellants, Explos. Pyrotech.*, **2005**, *30*, 5–16. [Crossref], [Google Scholar], [Publisher]
[27] O.S. Adeyemi, C.A. Otuechere, A. Adewuyi, A.A. Adeyanju, O.J. Awakan, D.A. Otohinoyi, *Nanoengineered Biomaterials for Advanced Drug Delivery*, **2020**, 329-345. [Crossref], [Google Scholar], [Publisher]
[28] C. Bengtsson, Synthesis of Substituted Ring- Fused 2-Pyridones and Applications in Chemical Biology, Ph.D. Dissertation, Umeå Universitet, **2013**. [Google Scholar], [Publisher]
[29] R.A.M.A.L. Hassani, S.A.H. Abdullah, S.K. Ibrahim, *Int. J. Chem. Sci.*, **2016**, *14*, 1939–1958. [Google Scholar], [PDF]
[30] H. Abbas, R. Al-hassani, *International Journal of Medical Science and Dental Research.*, **2018**, *01*, 1–2. [Google Scholar], [Publisher]
[31] M.F. Alias, M.M. Abdul Hassan, S.J. Khammas, *Int. J. Sci. Res.*, **2015**, *4*, 2337–2342. [Pdf], [Google Scholar], [Publisher]
[32] M.R. Aouad, D.J.O. Khan, M.A. Said, N.S. Al-Kaff, N. Rezki, A.A. Ali, N. Bouqellah, M. Hagar, *Chemistry Select*, **2021**, *6*, 3468–3486. [Crossref], [Google Scholar], [Publisher]
[33] P. Sharma, N.P. Kumar, K.R. Senwar, O. Forero-Doria, F.M. Nachtigall, L.S. Santos, N. Shankaraiah, *J. Braz. Chem. Soc.*, **2017**, *28*, 589–597. [Crossref], [Google Scholar], [Publisher]
[34] K. Gonzalez-silva, D. Rendon-nava, A. Alvarez-herna, D. Mendoza-espinosa, *New J. Chem.*, **2019**, *42*, 16538–16545. [Crossref], [Google Scholar], [Publisher]
[35] L. Zheng, Y. Wang, X. Meng, and Y. Chen, *Catal. Commun.*, **2021**, *148*, 106165. [Crossref], [Google Scholar], [Publisher]
[36] C. Anitha, S. Sumathi, P. Tharmaraj, C.D. Sheela, *Int. J. Inorg. Chem.*, **2011**, 1-8 [Crossref], [Google Scholar], [Pdf]
[37] F.I. Abouzayed, S.M. Emam, S.A. Abouel-Enein, *J. Mol. Struct.*, **2020**, *1216*, 128314. [Crossref], [Google Scholar], [Publisher]
[38] S.S. Kumari, *Asian J. Chem.*. **2020**, *32*, 192-194. [Crossref], [Pdf], [Publisher]

How to cite this article: Jihan Hameed Abdulameer, Mahasin F. Alias. Synthesis and characterization of some metal complexes with 2,6-bis(((1-octyl-1H-1,2,3-triazol-4-yl) methoxy) methyl) pyridine and the study of their biological activities. *Eurasian Chemical Communications*, 2022, 4(12), 1266-1284. **Link:** http://www.echemcom.com/article_153876.html